



# Effects of the precursor concentration and different annealing ambients on the structural, optical, and electrical properties of nanostructured $V_2O_5$ thin films deposited by spray pyrolysis technique

Rowshanak Irani<sup>1</sup> · Seyed Mohammad Rozati<sup>1</sup> · Szabolcs Beke<sup>2</sup>

Received: 31 July 2017 / Accepted: 14 March 2018 / Published online: 19 March 2018  
© Springer-Verlag GmbH Germany, part of Springer Nature 2018

## Abstract

$V_2O_5$  thin films were deposited with different precursor concentrations of 0.01, 0.05, and 0.1 M on glass substrates by spray pyrolysis technique, then the optimized films were annealed in different ambients (air, oxygen, and vacuum). The results showed that by increasing the concentration, the films grew along the (001) direction with an orthorhombic structure. Field emission scanning electron microscopy showed that nanorods were formed when depositing 0.05 molar of  $VCl_3$ . We conclude that with the precursor concentration, the surface nanostructure can be well-controlled. Annealing improved the crystallinity under all ambients, but the best crystallinity was achieved in vacuum. It was revealed that the as-deposited films had the highest transmission, whereas the films annealed in air had the lowest. When annealed in air, the optical band gap decreased from 2.45 to 2.32 eV. The sheet resistance, resistivity, mobility, conductivity, and carrier concentration were measured for all the prepared  $V_2O_5$  films.

## 1 Introduction

The transition metal oxide semiconductors offer a wide range of applications due to their unique properties. Vanadium pentoxide has drawn significant interest among these various metal oxides over the past few decades [1]. High electrochemical activity, stability, and ease of thin film formation by numerous deposition techniques are the characteristics that led to its use as a highly promising intercalation material for applications [2] in a wide range of microelectronic [3], electrochemical [4], and optoelectronic [5, 6] devices. It has also been used as catalyst [7], gas sensor [8, 9], window for solar cells [10], electrochromic devices [11, 12], and for the fabrication of thin film batteries [13]. Some more delicate examples of  $V_2O_5$  applications are gained in its conjunction with molybdenum [14] and tungsten oxides [15] for charge-balanced devices for display production in

informatics, variable reflection mirrors, smart windows in energy efficient architecture, and selective  $H_2$  sensors [9, 16].

Virtually, all deposition techniques [1] have been used to prepare  $V_2O_5$  thin films, such as radio frequency sputtering [17], dc-magnetron sputtering [18], flash evaporation [19], sol-gel technique [20], plasma-enhanced chemical vapor deposition [21], pulsed laser deposition [22–25], and spray pyrolysis [6, 26].  $V_2O_5$  crystallizes with an orthorhombic unit cell structure with lattice parameters of  $a = 12.286 \pm 0.627 \text{ \AA}$ ,  $b = 3.548 \pm 0.029 \text{ \AA}$  and  $c = 4.39 \pm 0.033 \text{ \AA}$  [26]. The deposition temperature directly influences the crystallization of the films [26], which depends both on the deposition technique and the phase (crystalline or amorphous) of the substrate material [1]. Vanadium oxide thin films are amorphous when deposited at substrate temperatures less than  $300 \text{ }^\circ\text{C}$  [1, 25].  $V_2O_5$  is the most stable oxide in the V–O system inasmuch, as it is the saturated one among  $VO_2$ ,  $V_4O_9$  and all of other oxides of vanadium [1].

In our previous work [26], we have extensively studied the sprayed  $V_2O_5$  thin films deposited at different substrate temperatures, i.e., their structural and optical properties, the morphology of films, and the optimization of growth

✉ Seyed Mohammad Rozati  
smrozati@guilan.ac.ir

<sup>1</sup> Department of Physics, University of Guilan, Rasht, Guilan 41335, Iran

<sup>2</sup> Department of Nanophysics, Istituto Italiano di Tecnologia (IIT), 16163 Genoa, Italy

temperature. The X-ray diffraction (XRD) data have been used to calculate the lattice parameters. From the field emission scanning electron microscopy (FESEM) results, the mean size of the nanorods' diameters has been determined and found to be around 40 nm. The direct forbidden optical band gap was calculated to be 2.1 eV for the films deposited at optimized deposition conditions.

In this paper, the effect of precursor concentration and thermal annealing in three different ambients are investigated. First,  $V_2O_5$  thin films with different molarities of precursor concentration have been deposited on glass substrates by a spray pyrolysis technique. Then, the optimized films were annealed at 200 °C for 1 h in air, oxygen (with flow rate of 1 l/min.), and vacuum of  $10^{-5}$  Torr. The variations in the structural, optical, and electrical properties as a function of thermal annealing were investigated. The absorption edges and the optical band gaps are estimated using the Tauc plot and it showed a decrease for all annealed films compared with the as-deposited ones. To our knowledge, it is the first time that the annealed  $V_2O_5$  films are being investigated in various ambients. The novelty of this work is that the physical properties of the  $V_2O_5$  thin films before and after annealing is widely studied. There has been no other works concentrating on these excellent properties such as the change in the band gap of the films, which is a very crucial factor in many applications. The basic concepts of physical properties of vanadium pentoxide films have been investigated in the paper that can be used for further usages in the mentioned applications.

## 2 Experimental procedures

Different concentrations (0.01, 0.05, and 0.1 M) of  $VCl_3$  powder (96%, purchased from Fluka) in 40-cm<sup>3</sup> double-distilled water were used as precursor solution. Compressed and filtered airflow with a rate of 16 l/min was used as carrier gas. It carried solution particles to the heated glass substrates that were cleaned with water, rare nitric acid, acetone, and then immersed in ultrasonic bath. The nozzle-substrate distance was 25 cm. Optimized thin films deposited by the above-mentioned deposition parameters were then annealed at 200 °C in air, oxygen, and vacuum for 1 h. Chemical vapor deposition (CVD) was applied for annealing the films in the specified flow of air and oxygen. Further annealing in vacuum was done in a vacuum chamber.

XRD was used to reveal the structural characterizations of the films using a Philips PW 1800 powder diffractometer using Ni-filtered  $Cu-K_\alpha$  radiation (0.15406 nm). The Scherrer's formula of  $D = K\lambda/(\beta\cos\theta)$  was exerted to calculate the mean size of crystallites ( $D$ ) from the full-width at half-maxima (FWHM) of the corresponding X-ray diffraction peaks, where  $K$  is a constant depending on the particle

shape (in this case  $K=0.9$ ),  $\lambda$  is the wavelength of the X-ray radiation,  $\beta$  is the FWHM which was found using origin software and  $\theta$  is the angle of reflection. To investigate the optical properties transmission measurements were performed by Cary 100 scan UV–visible spectrophotometer. Diffuse transmission and reflectance measurements were performed by an AvaSpec2048Tec spectrometer (Avantes) to investigate the optical properties. The electrical properties were studied using a RH2010 (PhysTech) Van der Pauw and Hall Effect measurement system. The thicknesses of films were calculated by applying the  $R = \rho/t$  equation from the Hall measurements. The manufacturer's (Microstructure measurement) and a commercial (X'pert, Origin) software were used for data analyzing. The morphology of thin films was observed by field emission scanning electron microscopy (FESEM) using a Hitachi S4160 (Hitachi Japan). To provide better electrical conductivity, a thin film of Au was sputtered on the samples prior to the SEM observations.

## 3 Results and discussion

### 3.1 X-ray diffraction measurement

The deposition parameters, except the precursor solution, were kept constant. Figure 1 shows a set of XRD patterns of  $V_2O_5$  thin films deposited with 0.01, 0.05, and 0.1 molar (M) of precursor concentration. First, the films deposited with 0.01 M revealed the (241) direction as the dominant peak at  $2\theta \approx 28.9$ . This peak corresponds to the tetragonal  $V_2O_5$  phase (ICCD data No 45-1074 card) confirming the low precursor concentration leading to the formation of  $V_2O_5$  films with a tetragonal symmetry in the structure.

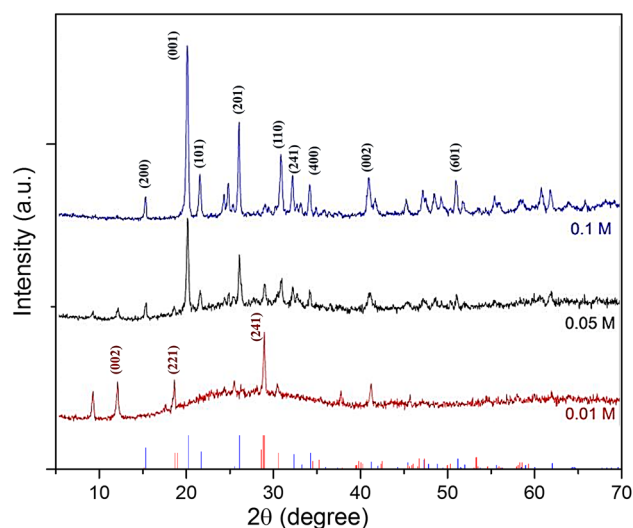


**Fig. 1** X-ray diffraction patterns of sprayed  $V_2O_5$  thin films deposited with 0.01, 0.05, and 0.1 M of precursor

It is clearly visible that the orientations become preferred along the (001) direction by increasing the concentration. The pattern reveals the polycrystalline structure with the predominant (001) peak of orthorhombic  $V_2O_5$  phase for the films prepared with 0.05 M. By increasing the precursor concentration to 0.1 M, all the peaks increased as well as the (001) peak. Thus, by further increasing the precursor concentration just the thickness was increased. Therefore, the 0.05 M was chosen as the optimum concentration and the films prepared from 0.05 M precursor concentration were employed in various ambients under annealing. Figure 2 shows a set of XRD patterns of  $V_2O_5$  as-deposited films (prepared from 0.05 M of  $VCl_3$ ), annealed in oxygen, air, and vacuum ambients. The peaks were indexed based on the  $V_2O_5$  powder file (ICCD data No 41-1426) corresponding to the Pmmn space group of orthorhombic symmetry. The peaks located at  $2\theta \approx 20.2^\circ$ ,  $21.5^\circ$ ,  $41^\circ$  assume the orthorhombic  $V_2O_5$  phase which are assigned to the (001), (101) and (002) reflections, respectively [22, 27, 28]. The pattern of the as-deposited films reveals the polycrystalline structure with the predominant (001) peak. In the same XRD spectrum, relatively low (200) and (241) peaks corresponding to the tetragonal  $V_2O_5$  phase are also present confirming the presence of  $V_2O_5$  also with tetragonal symmetry in the structure [2]. The XRD patterns of the annealed films show the same phases, but the peaks become sharper, particularly the films annealed in vacuum. Consequently, annealing the films yields more crystallized films and causes the formation of larger clusters. Table 1 shows the crystallite sizes corresponding to an average crystallite size around the (001) direction. It can be concluded that each oxide film has a nanocrystalline structure.

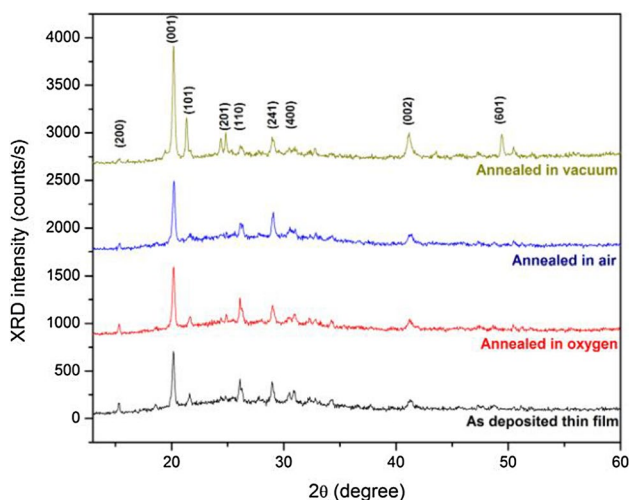


**Fig. 2** X-ray diffraction patterns of sprayed  $V_2O_5$  thin films deposited in a 16 l/min gas flow rate and 0.05 M of precursor, and annealed in air, oxygen and vacuum for 1 h at  $200^\circ C$

### 3.2 Optical diffuse transmission, reflectance, and band gap calculations

By increasing the precursor solution, the transparency of the films decreased (Fig. 3) which can be due to the increase in thickness. This can also be observed in the FESEM results.

**Table 1** Crystallite sizes as a function of the annealing ambient

Sample	As-deposited	Annealed in oxygen	Annealed in vacuum	Annealed in air
Crystallite size (nm)	29.4	28.8	29.1	27.3

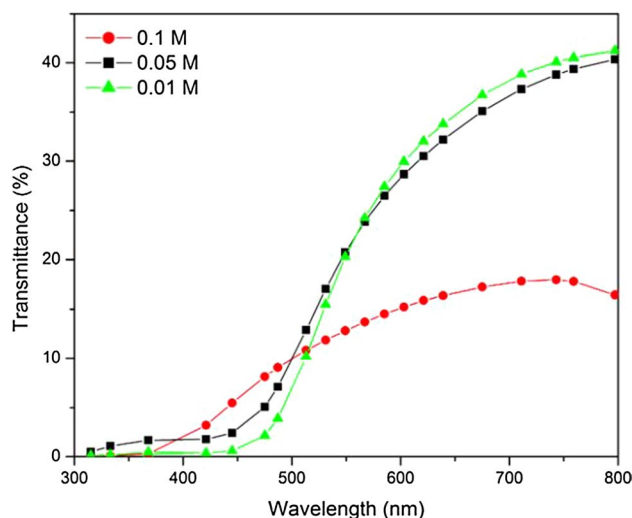


**Fig. 3** Optical transmission characteristics of  $V_2O_5$  thin films deposited with different precursor concentrations

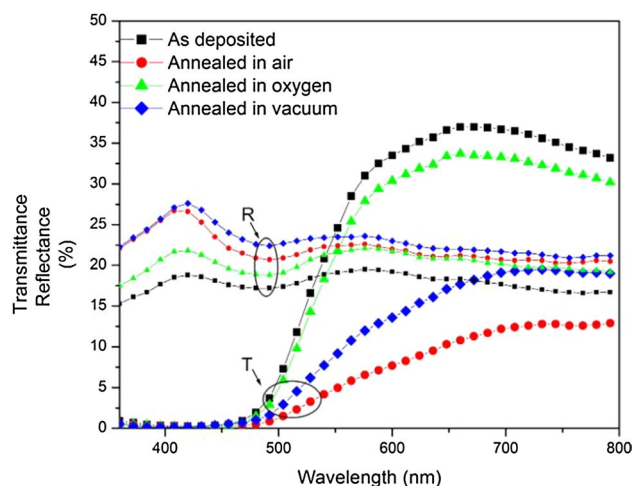


**Fig. 4** Diffuse transmittance and reflectance characteristics of  $V_2O_5$  as-deposited thin films, and annealed in air, oxygen, and vacuum, the precursor concentration was 0.05 M for all

The variation in the spectral transmittance and reflectance for the films with 0.05 M concentration is shown in Fig. 4. The as-deposited films had the highest transmission, while the films annealed in air had the lowest. Presumably, the porosity of the films has decreased by the oxygen adsorption during annealing, thus the extinction coefficient increased causing a lower transmission. The optical band gap can be estimated using Eqs. 1 and 2. From the measured transmittance and reflectance spectra, the optical absorption coefficient of the films was derived using the Eq. 1.

$$\alpha = [1/t] \ln \{T/(1 - R)^2\}, \tag{1}$$

where  $T$  is the transmittance,  $R$  is the reflectance, and  $t$  is the thickness of the film (thickness values were evaluated to be around 900 nm for the films before and after annealing). We can evaluate the optical band gap using the revealed absorption coefficient and solving the Eq. 2.

$$\alpha h\nu = B(h\nu - E_g)^n, \tag{2}$$

where  $h\nu$  is the incident photon energy,  $B$  is the edge width parameter,  $E_g$  is the band gap, and  $n$  is the exponent which can take values depending on the type of electronic transition causing the absorption. Then, by applying the Tauc plot and plotting  $(\alpha h\nu)^{1/n}$  vs.  $h\nu$  (Fig. 5), the optical band gap can be evaluated by extrapolating the linear region of the plot to zero ( $\alpha = 0$ ) [1, 22]. There are different values for the electron transition causing the absorption for the exponent  $n$ . The values 1/2, 3/2, 2, 3 correspond to direct allowed, direct forbidden, indirect allowed, and indirect forbidden transitions, respectively [22, 29].

As it is shown in Fig. 5 the 2/3 (direct forbidden) fit gives reasonable results for the absorption edge. It is visible that the band gap decreased from 2.45 to 2.32 eV when annealed in air. This band gap decrease with annealing agrees well with the Brus model of the energy gap confinement effect in nanostructured semiconducting materials [30]. This blue shift in the band gap values in case of annealing  $V_2O_5$  thin films has not been reported elsewhere, but these values are in an agreement with the literature. The band gap was reported

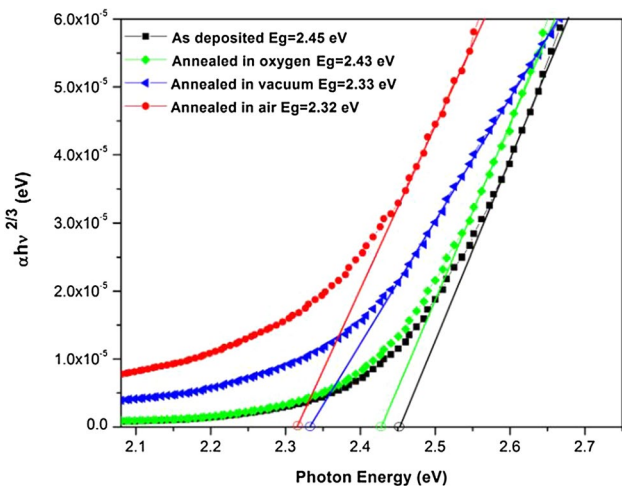


Fig. 5  $(\alpha h\nu)^{1/n}$  vs.  $h\nu$  plots for  $V_2O_5$  as-deposited thin film, and annealed in air, oxygen, and vacuum

Table 2 Sheet resistance, resistivity, mobility, carrier concentration, and conductivity type obtained by Hall effect

Annealing ambient	Sheet resistance ( $\Omega/\text{cm}^2$ )	Resistivity ( $\Omega \text{ cm}$ )	Mobility ( $\text{cm}^2/\text{V s}$ )	Conductivity type	Carrier concentration ( $\text{cm}^{-3}$ )
As-deposited	$1.57 \times 10^{+4}$	$1.41 \times 10^{00}$	$5.20 \times 10^{+01}$	$n$	$8.49 \times 10^{16}$
Annealed in air	$1.61 \times 10^{+4}$	$1.45 \times 10^{00}$	$7.66 \times 10^{-02}$	$n$	$5.64 \times 10^{20}$
Annealed in oxygen	$3.30 \times 10^{+4}$	$2.97 \times 10^{00}$	$6.51 \times 10^{-02}$	$n$	$3.23 \times 10^{19}$
Annealed in vacuum	$1.61 \times 10^{+4}$	$1.45 \times 10^{00}$	$3.59 \times 10^{00}$	$n$	$1.20 \times 10^{18}$

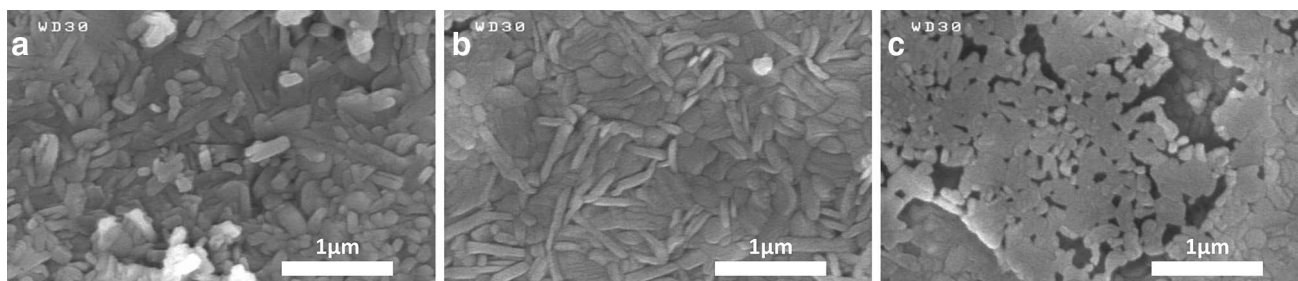


Fig. 6 FESEM images of thin films deposited with a 0.01, b 0.05, and c 0.1 molar of precursor concentration

in the range 2.12–2.47 eV for thin films deposited by pulsed laser ablation [1, 29, 31]. A. A. Akl reported 2.33 eV for band gap of films deposited by spray pyrolysis technique [17], but 2.1 eV was also reported for the same technique [25]. There were similar values for the band gap of  $V_2O_5$  films deposited by pulsed laser deposition [1, 22, 24]. The optical band gap can vary from 2.04 to 2.66 eV for  $V_2O_5$  thin films as reported in a comprehensive review of optical band gaps for all deposition techniques of  $V_2O_5$  [1].

### 3.3 Electrical properties

The Hall effect results are shown in Table 2. The increase of the sheet resistance can be associated with the oxygen adsorption to the film by filling the vacancies. The oxygen vacancy plays an important role in the electrical conductivity [32]. It is clear that the annealing increases the carrier concentration, while decreases the mobility and the resistivity remains constant, which are the expected results as given in Eq. 3 [33].

$$\rho = 1/Ne\mu, \quad (3)$$

where  $N$  is the carrier concentration,  $e$  is elementary electric charge, and  $\mu$  is the carrier mobility. The as-deposited  $V_2O_5$  thin films and the annealed ones have  $n$ -type conductivity (revealed from the Hall effect), which is in agreement with other reports [34, 35].

### 3.4 Field emission scanning electron microscopy

The morphology of the films was determined using field emission scanning electron microscopy (Fig. 6). The results revealed that nanorods were formed. It is visible that by increasing the precursor concentration a homogeneous surface forms and by a further increase, some defects occur on the surface of the film, which can be associated with the thickness increase. The morphology of  $V_2O_5$  as-deposited thin films with the precursor concentration of 0.05 M and annealed ones (with the same concentration) in different ambients is shown in Fig. 7. These results reveal that nanorods have been formed on the as-deposited films' surface. Similarly, nanorods are visible on the surfaces of the annealed films, but their numbers decreased and they became larger. The images also show more smoothness for the annealed films. Figure 8 presents the diameter size distribution corresponding to the as-deposited and the annealed films (all with the optimized precursor concentration of 0.05 M). The diameters of nanorods vary between 3 and

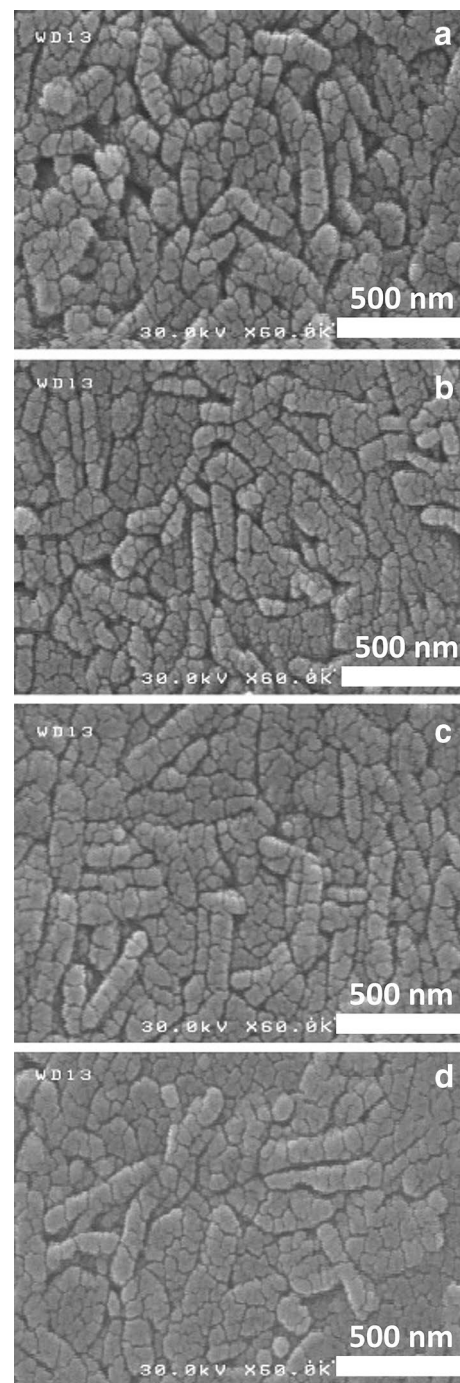


**Fig. 7** FESEM images of the **a** as-deposited thin films with the optimized  $VCl_3$  concentration of 0.05 M, **b** post-annealed in air, **c** post-annealed in oxygen, and **d** post-annealed in vacuum

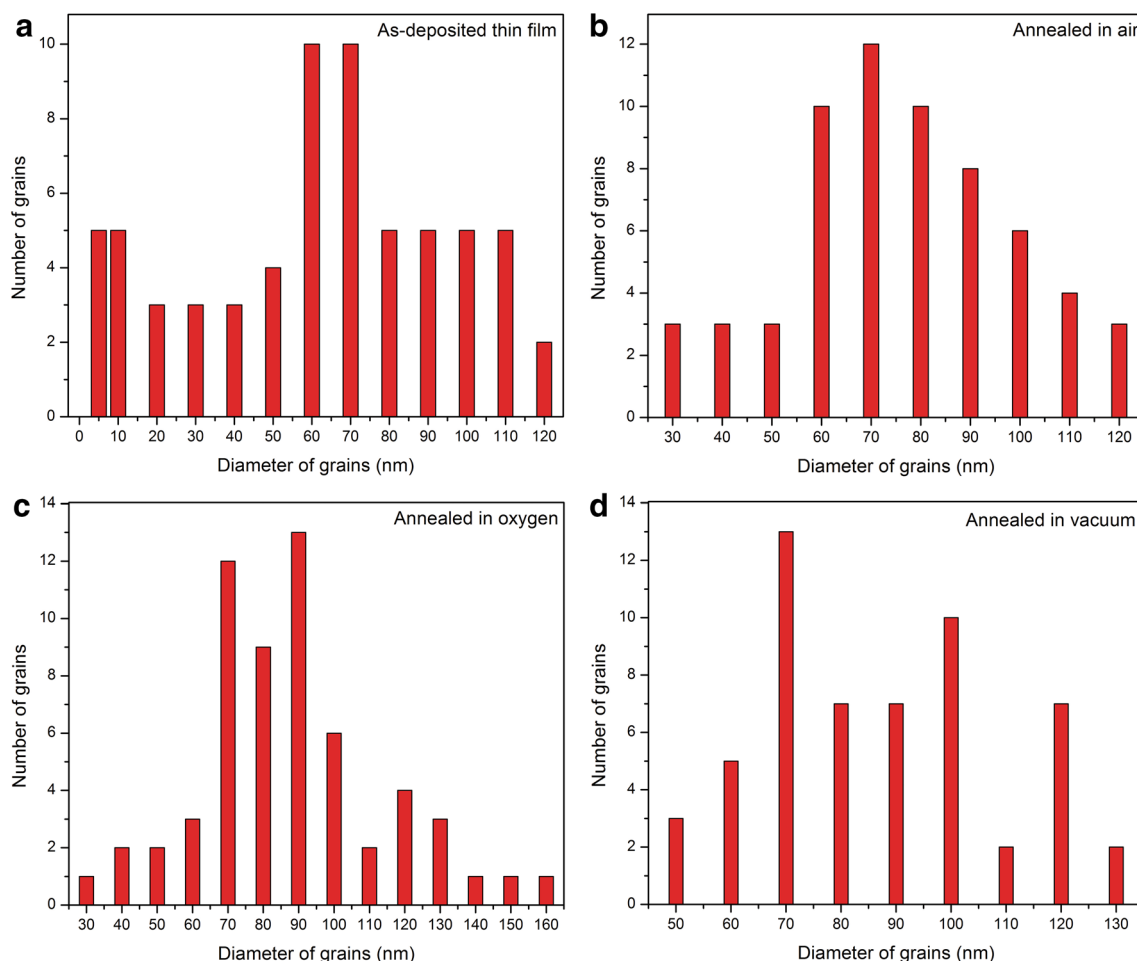


**Fig. 8** Distribution of the grains diameters; **a** as-deposited thin films (0.05 M  $VCl_3$ ), **b** post-annealed in air, **c** post-annealed in oxygen, and **d** post-annealed in vacuum

160 nm. The nanorods of the as-deposited films have a diameter of about 65 nm that is shorter than those of the annealed ones. The length distribution graphs for the as-mentioned thin films are shown in Fig. 9 indicating that the rods on the surfaces of the annealed films are longer. FESEM observations give accurate measurements of the grain sizes and provide an excellent analysis of the films' surfaces.

## 4 Conclusions

A spray pyrolysis technique was employed to deposit  $VCl_3$  powder with different concentrations on glass surfaces. Changing the concentration yielded a positive change in the orientations. By increasing the concentration, the films became thicker resulting in a lower transmission. The

crystallite sizes were evaluated and it resulted in about 30-nm-sized grains. Then, the optimized films with 0.05 M precursor concentration were annealed in different ambients (air, oxygen, and vacuum). The thin films were verified as nanostructured  $V_2O_5$  with orthorhombic unit cell structure using X-ray diffraction. The mean grain diameters of the as-deposited films were approximated about 65 nm, indicating that the diameters grew after annealing. The optical properties of the films were studied using diffuse transmission and reflectance measurements. The Tauc plot revealed that when annealed in air, the direct forbidden band gap decreased from 2.45 to 2.32 eV, which can be explained by the Brus model. Studying the electrical properties showed that filling the vacancies by oxygen atoms during annealing causes an increase in the sheet resistance. The sheet

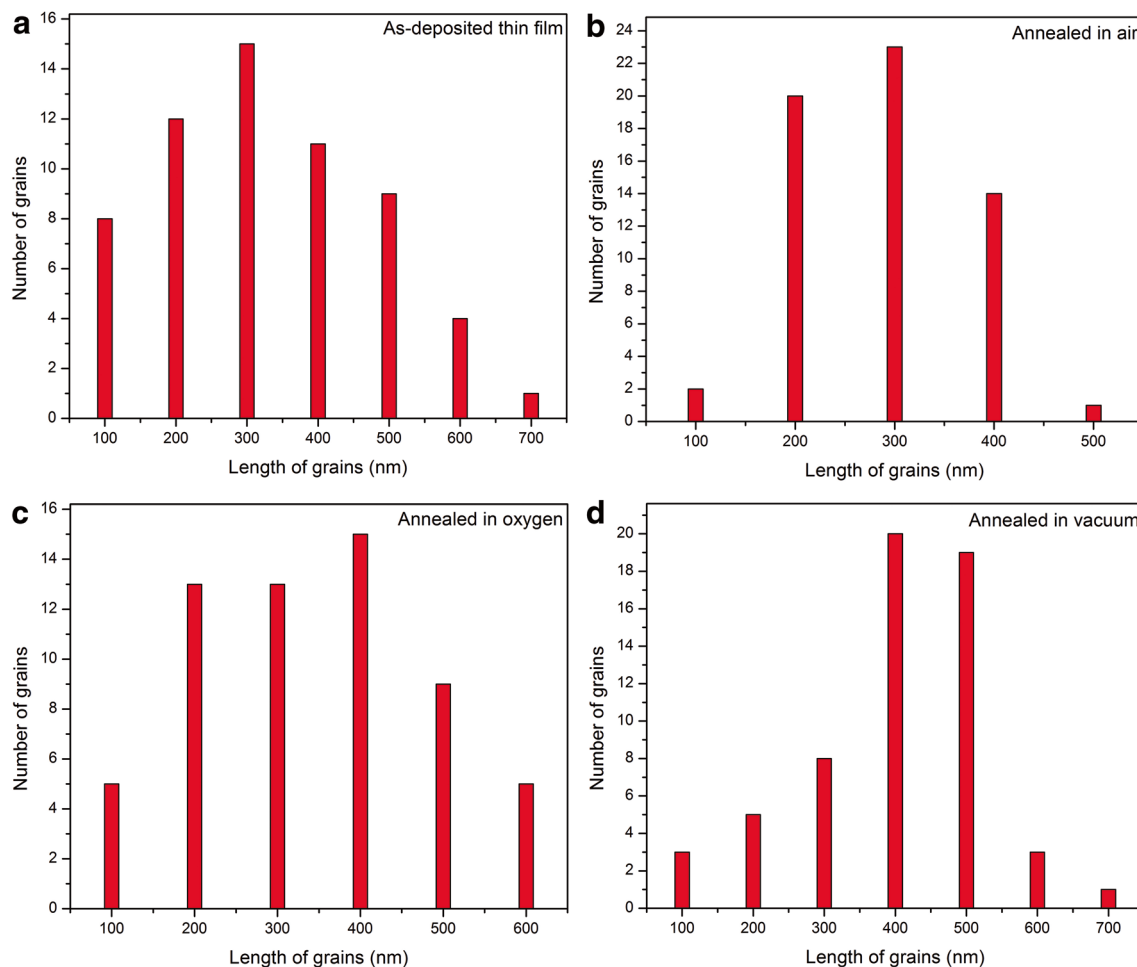


**Fig. 9** Distribution of the grains lengths; **a** as-deposited thin films (0.05 M  $VCl_3$ ), **b** post-annealed in air, **c** post-annealed in oxygen, and **d** post-annealed in vacuum

resistance, resistivity, mobility, conductivity, and carrier concentration were calculated for all prepared  $V_2O_5$  films.

**Acknowledgements** The authors gratefully acknowledge the research department of University of Guilan.

## References

1. S. Beke, A review of the growth of  $V_2O_5$  films from 1885 to 2010. *Thin Solid Films* **519**, 1761–1771 (2011)
2. A. Bouzidi, N. Benramdane, S. Bresson, C. Mathieu, R. Desfeux, M. El Marssi, X-ray and raman study of spray pyrolysed vanadium oxide thin films. *Vib. Spectrosc.* **57**, 182–186 (2011)
3. K.A. Cook-Chennault, N. Thambi, A.M. Sastry, Powering MEMS portable devices—a review of non-regenerative and regenerative power supply systems with special emphasis on piezoelectric energy harvesting systems. *Smart Mater. Struct.* **17**, 043001–043034 (2008)
4. M.B. Sahana, C. Sudakar, C. Thapa, G. Lawes, V.M. Naik, R.J. Baird, G.W. Auner, R. Naik, K.R. Padmanabhan, Electrochemical properties of  $V_2O_5$  thin films deposited by spin coating. *Mater. Sci. Eng. B* **25**, 42–50 (2007)
5. G.J. Fang, Z.L. Liu, Y.Q. Wang, H.H. Liu, K.L. Yao, Orientated growth of  $V_2O_5$  electrochromic thin films on transparent conductive glass by pulsed excimer laser ablation technique. *J. Phys. D Appl. Phys.* **33**, 3018–3021 (2000)
6. A.A. Akl, Thermal annealing effect on the crystallization and optical dispersion of sprayed  $V_2O_5$  thin films. *J. Phys. Chem. Solids* **71**, 223–229 (2010)
7. V.I. Pârvulescu, S. Boghosian, V. Pârvulescu, S.M. Jung, P. Grange, Selective catalytic reduction of NO with  $NH_3$  over mesoporous  $V_2O_5$ - $TiO_2$ - $SiO_2$  catalysts. *J. Catal.* **217**, 172–185 (2003)
8. M. Abbasi, S.M. Rozati, R. Irani, S. Beke, Synthesis and gas sensors behavior of nanostructure  $V_2O_5$  thin films prepared by spray pyrolysis method. *Mater. Sci. Semicond. Process.* **29**, 132–138 (2015)
9. S.M. Kanan, O.M. El-Kadri, I.A. Abu-Yousef, M.C. Kanan, Semiconducting metal oxide based sensors for selective gas pollutant detection. *Sensors* **9**, 8158–8196 (2009)

10. S.S. Kanu, R. Binions, Thin films for solar control applications. *Proc. R. Soc. A* **466**, 19–44 (2010)
11. F. Bétique, J. Livage, Optical switching in VO<sub>2</sub> thin films. *J. Sol Gel. Sci. Technol.* **13**, 915–921 (1998)
12. Y. Wang, G. Cao, Li<sup>+</sup>-intercalation electrochemical/electrochromic properties of vanadium pentoxide films by sol electrophoretic deposition. *Electrochim. Acta* **51**, 4865–4872 (2006)
13. D. Alamarguy, J.E. Castle, M. Liberatore, F. Decker, Distribution of intercalated lithium in V<sub>2</sub>O<sub>5</sub> thin films determined by SIMS depth profiling. *Surf. Interface Anal.* **38**, 847–850 (2006)
14. T.J. Hanlon, J.A. Coath, M.A. Richardson, Molybdenum-doped vanadium dioxide coatings on glass produced by the aqueous sol–gel method. *Thin Solid Films* **436**, 269–272 (2003)
15. A. Rougier, A. Blyr, Electrochromic properties of vanadium tungsten oxide thin films grown by pulsed laser deposition. *Electrochim. Acta* **46**, 1945–1950 (2001)
16. C. Imawan, H. Steffes, F. Solzbacher, E. Obermeier, Structural and gas-sensing properties of V<sub>2</sub>O<sub>5</sub>–MoO<sub>3</sub> thin films for H<sub>2</sub> detection. *Sens. Actuators B* **77**, 346–351 (2001)
17. A.A. Akl, Crystallization and electrical properties of V<sub>2</sub>O<sub>5</sub> thin films prepared by RF sputtering. *Appl. Surf. Sci.* **253**, 7094–7099 (2007)
18. H. Poelman, H. Tomaszewski, D. Poelman, L. Fiermans, R. De Gryse, M.F. Reyniers, G.B. Marin, V<sub>2</sub>O<sub>5</sub> thin films deposited by means of d.c. magnetron sputtering from ceramic V<sub>2</sub>O<sub>3</sub> targets. *Surf. Interface Anal.* **34**, 724–727 (2002)
19. S. Guimond, J.M. Sturm, D. Goebke, Y. Romanyshyn, M. Naschitzki, H. Kuhlenbeck, H.J. Freund, Well-ordered V<sub>2</sub>O<sub>5</sub> (001) thin films on Au (111): growth and thermal stability. *J. Phys. Chem.* **112**, 11835–11846 (2008)
20. S. Beke, L. Kőrösi, S. Papp, L. Nánai, J.G. Kiss, V. Safarov, Nd:YAG laser synthesis of nanostructural V<sub>2</sub>O<sub>5</sub> from vanadium oxide sols: morphological and structural characterizations. *Appl. Surf. Sci.* **254**, 1363–1368 (2007)
21. D. Barreca, L. Armelao, F. Caccavale, V. Di Noto, A. Gregori, G.A. Rizzi, E. Tondello, Highly oriented V<sub>2</sub>O<sub>5</sub> nanocrystalline thin films by plasma-enhanced chemical vapor deposition. *Chem. Mater.* **12**, 98–103 (2000)
22. S. Beke, S. Giorgio, L. Kőrösi, L. Nánai, W. Marine, Structural and optical properties of pulsed laser deposited V<sub>2</sub>O<sub>5</sub> thin films. *Thin Solid Films* **516**, 4659–4664 (2008)
23. Y. Iida, H. Takashima, Y. Kanno, Optical and electrical properties of V<sub>2</sub>O<sub>5</sub> thin films fabricated by pulsed laser deposition. *Jpn. J. Appl. Phys.* **47**, 633–636 (2008)
24. S. Beke, L. Kőrösi, S. Papp, A. Oszkó, L. Nánai, XRD and XPS analysis of laser treated vanadium oxide thin films. *Appl. Surf. Sci.* **255**, 9779–9782 (2009)
25. S. Beke, L. Kőrösi, L. Nánai, F. Brandi, In-situ optical emission spectroscopy of laser-induced vanadium oxide plasma in vacuum. *Vacuum* **86**, 2002–2004 (2012)
26. R. Irani, S.M. Rozati, S. Beke, Structural and optical properties of nanostructural V<sub>2</sub>O<sub>5</sub> thin films deposited by spray pyrolysis technique: effect of the substrate temperature. *Mater. Chem. Phys.* **139**, 489–493 (2013)
27. C.Q. Feng, S.Y. Wang, R. Zeng, Z.P. Guo, K. Konstantinov, H.K. Liu, Synthesis of spherical porous vanadium pentoxide and its electrochemical properties. *J. Power Sources* **184**, 485–488 (2008)
28. A. Ashour, N.Z. El-Sayed, Physical properties of V<sub>2</sub>O<sub>5</sub> sprayed films. *J. Optoelectron. Adv. Mater.* **11**, 251–256 (2009)
29. C.V. Ramana, B.S. Naidu, O.M. Hussain, R. Pinto, Low-temperature growth of vanadium pentoxide thin films produced by pulsed laser ablation. *J. Phys. D Appl. Phys.* **34**, L35 (2001)
30. L.E. Brus, Electron–electron and electron–hole interactions in small semiconductor crystallites: the size dependence of the lowest excited electronic state. *J. Chem. Phys.* **80**, 4403–4409 (1984)
31. C.V. Ramana, R.J. Smith, O.M. Hussain, C.C. Chusuei, C.M. Julien, Correlations between growth conditions, microstructure, and optical properties in pulsed-laser deposited V<sub>2</sub>O<sub>5</sub> thin films. *Chem. Mater.* **17**, 1213–1219 (2005)
32. G.J. Fang, D. Li, B.L. Yao, Influence of post-deposition annealing on the properties of transparent conductive nanocrystalline ZAO thin films prepared by RF magnetron sputtering with highly conductive ceramic target. *Thin Solid Films* **418**, 156–162 (2002)
33. E.L. Wolf, M. Medikonda, *Understanding the Nanotechnology Revolution*, 1st edn. (Wiley-VCH, Weinheim, 2012)
34. A.D. Raj, T. Pazhanivel, P.S. Kumar, D. Mangalaraj, D. Nataraj, N. Ponpandian, Self-assembled V<sub>2</sub>O<sub>5</sub> nanorods for gas sensors. *Curr. Appl. Phys.* **10**, 531–537 (2010)
35. J. Woellenstein, J.A. Plaza, C. Cane, Y. Min, H. Boettner, H.L. Tuller, A novel single chip thin film metal oxide array. *Sens. Actuator B* **93**, 350–355 (2003)